Growth and patterning in vertebrate limb development
A timescale perspective on skeletal specification

S Ben Tahar, E Comellas, TJ Duerr, JR Monaghan, JJ Munoz, SJ Shefelbine

Contents

1 Abstract **2**

2 Introduction **2**

3 Results **3**
3.1 The Growth-Processing-Propagation model . . . 3
3.2 Integrating experimental data to predict axolotl limb patterning . . . 6

4 Discussion **7**
4.1 Growth as a missing link: bridging Turing patterns and positional information in whole limb patterning . . . 7
4.2 GPP and an evolutionary perspective . . . 8

5 Methods **8**
5.1 Growth . . . 8
5.1.1 Theory on growth . . . 8
5.1.2 Derivation of growth from experimental images . . . 9
5.2 Reaction-diffusion equation on growing domain . . . 10
5.2.1 Non-dimentionalization . . . 10
5.3 Numerical Simulations . . . 11
S0 Supplementary figures & tables . . . 16
S1.1 Table: Parameter selection for patterning simulations . . . 16
S2.2 Figures . . . 16
S0 Turing space through linear stability analysis . . . 17
S1.1 Derivation of the reaction-diffusion equation in a growing domain . . . 18
S2.2 Linear Stability Analysis in a growing domain . . . 19

1 Abstract

Skeletal patterning in limb development has historically been modeled resorting to two main approaches: positional information (PI) and reaction-diffusion (R-D) models. Although recent research has started to examine how they interact, the influence of growth in the models is still mostly ignored. In order to explicitly include growth as a key element of the patterning process, we propose a growth-reaction-diffusion framework.

Our model scales the system with the characteristic timescale of growth, introducing two key parameters: (1) the reaction time relative to growth and (2) the diffusion time relative to growth. Rather than modeling specific molecular pathways, we focus on the core processes that govern differentiation into cartilage. The reaction parameter represents information processing within the domain (e.g., protein production), while the diffusion parameter describes information propagation (e.g., signaling). Positional information informs the timescales of reaction and diffusion relative to growth.

To validate this framework, we simulate limb development in the mouse and axolotl. Our model reproduces established biological outcomes, including the effects of altered positional cues and morphogen distributions. We demonstrate that modulating the rate of specification processing and propagation relative to growth influences proximal-distal and anterior-posterior patterning.

By explicitly incorporating growth into a reaction-diffusion framework, our approach advances previous models and offers a more comprehensive understanding of limb skeletal patterning.

Significance

Skeletal patterning in limb development is a classic system to study morphogenesis. Numerical models have been informative for understanding how cells self-organize based on positional cues and local interactions to specify their fate. This study introduces the Growth-Processing-Propagation (GPP) framework, offering a new perspective on how growth modulates patterning through its influence on the relative speeds of processing and propagation of the specification information. The GPP framework bridges Turing's reaction-diffusion theory with Wolpert's positional information by incorporating growth as a key factor. It unifies the emergence of all limb segments –stylopod, zeugopod, and autopod– through a single, shared mechanism. This enables cross-species applicability, highlighting the framework's versatility in describing limb development across different organisms.

2 Introduction

The tetrapod limb serves as a powerful paradigm for studying organogenesis and to understand how developmental processes are coordinated. The developing limb is patterned along three primary axes: the proximodistal axis (PD), which is segmented into stylopod, zeugopod, and autopod, the anteroposterior axis (AP), which specifies the number of digits [1] and the dorsoventral axis (DV). Patterning along these axes has traditionally been attributed to two main signaling centers: the Apical Ectodermal Ridge (AER), which provides a distal cue guiding PD outgrowth and specification [2, 3], and the Zone of Polarizing Activity (ZPA), which controls AP identity and growth [4, 1]. Past studies indicate that these two centers do not function independently, but instead are part of a feedback loop [5, 6]. To explore these patterning mechanisms further, numerical simulations have served as an essential exploratory tool. They are primarily based on two theoretical frameworks: positional information and reaction-diffusion (Turing) system.

The traditional framework of positional information states that diffusible molecules, known as morphogens, form gradients that establish a coordinate system within the limb bud, giving a positional identity to cells [4]. These gradients could be regulated by sources located in the AER or the ZPA [7, 3, 8, 9]. Cells interpret specific morphogen concentrations to acquire their distinct fates. As an example of a gradient model, sonic hedgehog (Shh) signaling from the ZPA helps determine digit identity and number based on its concentration [8]. In the French flag model [4], positional identity follows a threshold-based mechanism, where different levels of morphogen exposure activate distinct genetic programs. The discovery of Hox genes provided a molecular basis for this idea [7]. These genes are activated in response to a morphogen

gradient, such as fibroblast growth factor from the AER or retenoic acid from the flank [10, 11, 12]. Hoxa9 is expressed throughout the limb, Hoxa11 in the zeugopod and stylopod, and Hoxa13 specifically in the autopod, together defining the identity of these three segments. The conservation of these expression patterns across tetrapods suggests that positional information acts as a shared blueprint for limb development that is sufficiently flexible to allow for variations in limb morphology [13]. While this model has been instrumental in explaining broad patterning mechanisms, it primarily addresses how cells acquire positional identity, rather than how the pattern within each skeletal element (e.g., digits) emerges.

In response to these limitations, there has been a renewed focus on Turing systems, or reaction-diffusion (R-D) models, as a mechanism to produce spatial patterns without predefined positional cues [14]. These models describe the interactions between two or more morphogens through coupled partial differential equations generating stable molecular patterns that guide cell fate. Recent progress has been made in identifying the gene regulatory networks driving these dynamics [15, 16]. However, gene regulatory networks are not static; key molecular players exhibit spatial and temporal context-dependent roles across developmental stages [5, 17, 18]. Furthermore, diffusion in reaction-diffusion models extends beyond simple morphogen transport, as receptor-mediated interactions have been shown to play a role in morphogen movement [19]. These findings call for a reinterpretation of the classical view of reaction-diffusion systems as fixed molecular interactions. Despite these limitations in their underlying assumptions, Turing-based numerical models have provided key insights into limb patterning, particularly digit periodicity [16, 20, 21, 22]. However, many of these models focus on individual limb segments or divide the limb into subdomains. This segmentation overlooks the interdependence of the proximal-distal and anterior-posterior axes as well as the influence of growth rate, highlighting the need to reconsider computational approaches.

Proper modeling of growth is necessary to understand pattern formation. Growth represents the continuous change in limb shape and size throughout development. Geometry influences the patterns generated by reaction-diffusion models [23]. However, in addition to accurately capturing changes in geometry, the model must account for how growth transports molecular signals within the tissue. Mathematically, this is translated into a convective term in the reaction-diffusion system, which depends on the growth rate [24]. Both aspects are needed to correctly model patterning within a growing domain. Some mathematical models incorporate growth into their equations, but are often solved in idealized, synthetic domains [25, 26, 27, 28]. In contrast, many studies with realistic biological geometries either neglect growth or fail to explore how growth rate influences the emergence of patterns [16, 20, 21, 22].

In this paper, we introduce a framework that integrates experimentally measured growth with the Turing system and positional information. We propose a model suggesting that positional information does not directly control molecular reactions but instead regulates the relative speed of reaction and diffusion with respect to growth. This shift allows to reinterpret reaction-diffusion systems as processing-propagation events, which we modulate within the different regions of the domain by modifying the relative rate of the reaction and diffusion terms in our equations with respect to concomitant growth rate. Our framework captures how different limb segments emerge continuously over time within an experimentally measured growing domain.

3 Results

3.1 The Growth-Processing-Propagation model

We propose a conceptual framework that models the specification of skeletal identity. Within this framework, u represents the specification identity for skeletal elements, while v represents an antagonist of this specification. As a result, the patterns generated in our model correspond to skeletal elements: the humerus, radius, ulna, and digits.

The reaction-diffusion model within a growing domain is interpreted as a Growth-Processing-Propagation (GPP) framework, introducing biologically meaningful interpretations to the system's components (Fig. 1A). In this framework, reaction corresponds to processing while diffusion is interpreted as propagation. Processing refers to the cellular mechanisms by which specification information is interpreted and acted upon. This may include transcriptional activation of genes, signal transduction cascades,

or other intracellular processes that regulate cell fate decisions. Propagation represents the transmission of specification information across the tissue. This can occur through the diffusion of signaling molecules or through direct cell-cell communication mechanisms, such as gap junctions or mechanical coupling. Growth in this context involves both cell proliferation and extracellular matrix production, which drive the shape changes of the limb bud throughout development. By incorporating growth, the framework mimics the evolving geometry of the limb development. Additionally, this integration produces a model where processing and propagation interact with growth through the parameters α_R and β_D to create patterns. To formalize this framework, we describe the Growth-Propagation-Processing system with the following equation:

$$\frac{d\mathbf{c}}{dt} + S(\mathbf{x},t)\,\mathbf{c} = \beta_D \mathbb{D}\,\nabla^2_{\Omega_x}\mathbf{c} + \alpha_R \mathbf{R}(\mathbf{c},\mathbf{x},t), \tag{1}$$

where $S(\mathbf{x},t)\,\mathbf{c}$ is the convective term accounting for growth, $\beta_D \mathbb{D}\,\nabla^2_{\Omega_x}\mathbf{c}$ represents propagation through a diffusion process, $\alpha_R \mathbf{R}(\mathbf{c},\mathbf{x},t)$ corresponds to processing (See section 5). The parameters α_R and β_D represent the relative timescales of growth to processing (reaction) and propagation (diffusion), respectively, and will be considered as imposed non-constant parameters that will help us to indicate the different regions of the whole domain. Values of these parameters below 1 indicate that growth outpaces the processing-propagation processes, while values above 1 suggest that processing-propagation occurs on a timescale faster than growth.

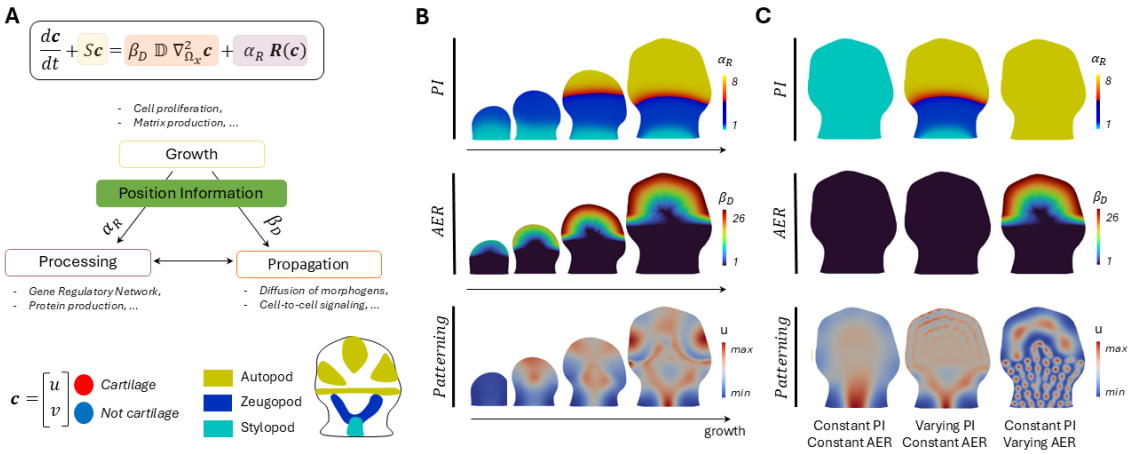

Figure 1. Computer simulation of skeletal patterning on a representative growing mouse limb bud. (**A**) The variable $\mathbf{c}$ represents the vector of the out-of-phase species, where high values of u indicate the differentiation of skeletal elements. The convective term $S\mathbf{c}$ captures the effect of growth, with S representing the growth rate. The diffusion term $\beta_D \mathbb{D} \nabla^2_{\Omega_x}\mathbf{c}$ represents propagation, and the reaction term $\alpha_R \mathbf{R}(\mathbf{c})$ represents processing. Growth, propagation, and processing refer to how cells interpret, transmit, and respond to patterning signals via tissue expansion, signaling spread and gene regulation. (**B**) The first row shows the input map of morphogens that provide Positional Information (PI) to each limb segment. In the model, this is represented by an increase in α_R. The second row displays the input map of the Apical Epithelial Ridge (AER) through an increase of β_D. The parameters α_R and β_D correspond to the relative timescales of processing and propagation relative to the growth. The final row shows the predicted skeletal patterning, with regions of high u values shown in red indicating locations of condensation. The humerus, followed by the radius and ulna, and, finally, five digits can be identified. (**C**) The columns are labeled C1, C2, C3. C1 represents the framework without incorporating PI or AER, resulting in a simple stripe pattern. C2 includes PI but excludes AER, preserving the proximal pattern seen in (B) but losing stripe orientation. C3 incorporates AER but excludes PI, leading to the loss of more proximal skeletal elements. The geometry shown is the final stage of growth.

The GPP framework enables us to bridge Turing's reaction-diffusion theory with Wolpert's positional information (PI) [4]. Positional information acts upstream of the GPP system, modulating the two key parameters that control the temporal relationship between growth, processing, and propagation. To achieve this, we vary the values of α_R and β_D in both space and time, with α_R increasing along the proximodistal axis and β_D exhibiting higher values in distal regions. As the limb bud grows and changes shape over time, these spatial variations in α_R and β_D become more pronounced. The parameter α_R controls the wavelength of the pattern, which determines the number of stripes (skeletal elements) formed (Fig. 1B). As α_R increases distally, the wavelength shortens, allowing a transition from one stripe (e.g., humerus)

to two stripes (e.g., radius and ulna) and eventually to multiple stripes (e.g., digits). Increasing α_R from proximal to distal suggests that distal regions process specification information faster relative to growth than the proximal regions. The variation of the parameter β_D governs the orientation of the stripe-like patterns, enabling alignment with distal cues, such as those provided by the AER. Higher β_D values in distal regions indicate faster propagation of specification information than proximal regions.

The absence of AER (Fig. 1C2) disrupts stripe orientation, highlighting the critical role of the AER in guiding pattern alignment for digit patterning. Including AER but excluding PI fails to produce realistic patterns for more proximal skeletal elements. In the absence of both PI and AER (Fig. 1C-1), the framework predicts simple stripe patterns, which potentially correspond to a rudimentary stylopod element.

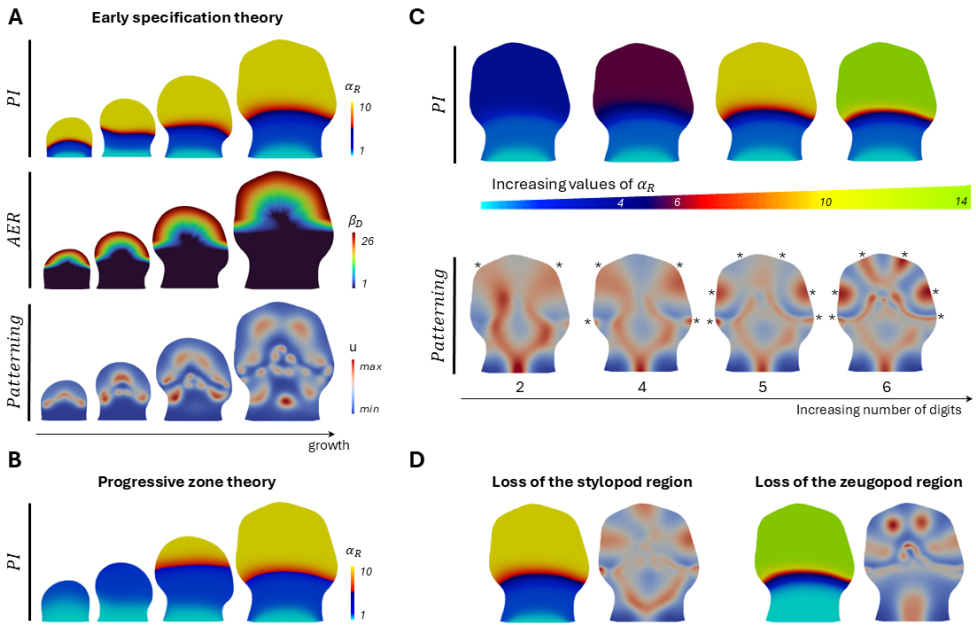

Figure 2. Exploring developmental concepts and testing theories: modifying and predicting limb segment outcomes with the GPP framework (**A**) The positional information is changed to match the early specification theory. (**B**) Positional information matching the progress zone theory as used for the simulation in Fig. 1B. Our model suggests that the specification of the three limb segments –stylopod, zeugopod, and autopod– occurs sequentially rather than being predetermined at the limb bud stage. (**C**) Only the final PI and pattern distribution is represented, which has been reached following the progress zone theory. Increasing the speed of processing relative to growth (controlled by the parameter α_R) in the autopod region leads to a greater number of digits. The stars indicates the digits. (**D**) Modifying the spatial boundaries of the stylopod or zeugopod regions using the values of α_R can result in the loss of proximal skeletal limb segments.

This conceptual framework allows us to explore two hypotheses in developmental biology: the progress zone model (Fig. 2B) and the early specification or expansion model (Fig. 2A). The progress zone model suggests that positional identity is acquired sequentially, with the stylopod forming first, followed by the zeugopod, and finally the autopod [29]. This is observed in Fig. 2B and 1B. In contrast, the early specification model proposes that all skeletal identities are established at the onset of limb bud formation. This is incorporated by having the gradient *stretch* with the domain growth. Patterning in Fig. 1B is as in the sketch of Fig. 1A, while in Fig. 2A the skeletal patterning is incorrect. This supports the progress zone model, as they indicate that specification unfolds progressively rather than being pre-determined.

Furthermore, this framework enables the investigation of positional information along both the proximal-distal and anterior-posterior axes. In our GPP framework, positional information is defined along the proximal-distal axis, but its coupling with the anterior-posterior axis emerges through the value of α_R. By adjusting the relative speed of processing compared to growth, we can modulate the number of digits formed, ranging from two to six (Fig. 2C). This reinforces the known interdependence between the two axes.

The framework cannot completely remove the stylopod or zeugopod without altering stylopod patterning (Fig. 2D). However, by shifting the transition points between different α_R values (cyan, blue and yellow regions in Fig. 2D), we can shorten specific segments disappear, in accordance with biological experi-

ments [30].

3.2 Integrating experimental data to predict axolotl limb patterning

To test the robustness of our framework across species, we applied it to the axolotl, an anamniote with well-documented differences in limb development compared to amniotes such as mice and chickens [31]. While several features of their development are unique, key principles are conserved. For instance, signaling centers like the AER and ZPA remain functionally present, and homeobox genes continue to play a central role in patterning [32, 33, 34, 35].

One of the most striking differences is that salamanders do not form a morphologically distinct apical ectodermal ridge. Instead, the epidermis exhibits AER-like properties without forming a thickened pseudostratified epithelium. Despite this, the AER retains its function [34]. Molecular signaling pathways also diverge in some aspects. For instance, while FGF8 is restricted to the apical ectodermal ridge in mice, in axolotls it initially appears in the epidermis and later shifts to the mesenchyme itself, with a pronounced anterior bias [36, 37]. This shift in localization suggests a divergence in the spatial dynamics of key signaling molecules, even as their roles in promoting limb outgrowth remain conserved. Another key difference lies in digit formation. In amniotes, digits form in a posterior-to-anterior sequence, through a paddle stage that is later sculpted by apoptosis in the interdigital regions [38]. In contrast, axolotl digits emerge in an anterior-to-posterior sequence, and the limb develops more through outgrowth of individual digits [31]. Despite these differences the fully patterned limb is remarkably similar. This raises the question whether the same underlying principles could be driving patterning in both systems, even if the specific signaling pathways may vary.

To explore this, the GPP framework was applied to axolotl limb development without altering the model structure. Only a few species-specific parameters were adjusted: the spatial magnitudes of α_R and β_D (SUPP. S1.1). The overall spatial trends are preserved, with both parameters increasing toward the distal tip of the limb. We model the positional information through an distal increase of α_R, as it was done for the mice. The positional information appears sequentially following the theory of the progress zone that has been shown experimentally in in axolotl limb development and regeneration [39, 40]. The AER influence is modeled the same way as in the mouse, with a distal increase of the values of β_D.

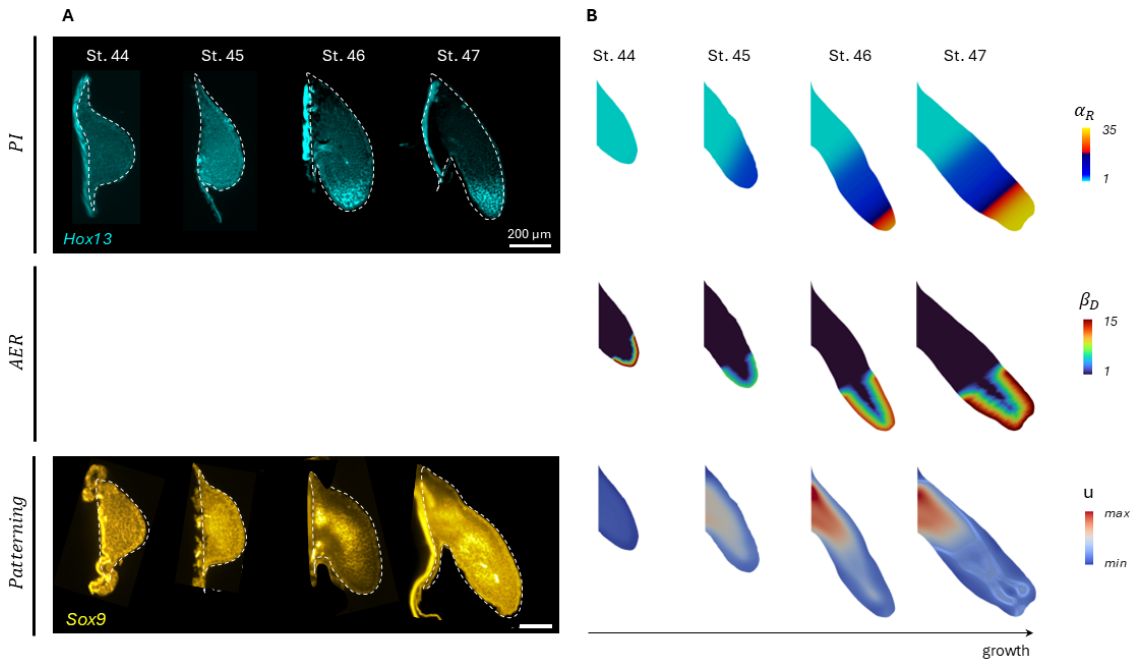

Figure 3. Axolotl limb patterning.
(**A**) Fluorescence imaging of Hoxa13 (top row) and Sox9 (bottom row) at different stages of limb development. (**B**) Numerical simulation using the GPP framework on experimentally measured geometry, with α_R and β_D as an input and u corresponding to the predicted skeletal patterning.

The limb geometries is extracted from experiments (Fig. 4). We also imaged key proteins at different

stages of development through fluorescence microscopy (Fig. 3A). The top row of Fig. 3A provides Hox13 expression to track the evolution of positional information. This enables us to inform the region of the digit positional information in the model (input). Finally, to validate numerical results (output), we imaged Sox9, which provides patterning corresponding to future cartilage condensation (Fig. 3A).

The model is able to reproduce the upper limb patterning in the axolotl, including the emergence of digit regions. The role of AER signaling and positional information is further explored in supplementary simulations (Fig. S1).

4 Discussion

4.1 Growth as a missing link: bridging Turing patterns and positional information in whole limb patterning

In this work, we introduce the Growth-Processing-Propagation (GPP) framework to provide a numerical tool for testing hypotheses in developmental biology. It is structured around three fundamental processes: 1) growth, which captures changes in size and shape; 2) processing, which includes gene regulatory interactions and their effects, such as reaction terms; and 3) propagation, encompassing morphogen signaling, cell-cell signaling, diffusion, etc. (Fig. 1A). Shifting the focus from explicit genetic networks to how the GPP system evolves over time and space allows us to examine the effects and influences of these three processes more conceptually.

By taking this approach, we reinterpret reaction-diffusion (R-D) and positional information (PI) interactions beyond gene regulatory networks and focus on broader self-organization principles. A gene regulatory network represents the network of a group of proteins that can determine cell fate [41]. Some candidates for digit patterning modeled through an R-D system include the Sox9-Bmp-Wnt feedback loop [16, 42] and the TGF-β-Bmp loop [43]. Similar to previous models that assume that positional information directly modifies molecular kinetics, our approach considers how positional cues regulate the speed of processing and propagation [20, 16]. However, our framework does not assume specific molecular pathways or how they are processed within the cell. This level of spatial and temporal continuity allows a systematic investigation of different segments of the limb interact, respond to perturbations, and influence one another over time (Fig. 2C,D). For example, we can assess how removing or modifying the AER and P-D cues affect the emergence of limb structures at different developmental stages (Fig. 1C). This perspective also allows exploring of fundamental developmental hypotheses, such as the distinction between the Progress Zone and Early Specification models (Fig. 1B, Fig. 2A).

One of the most fundamental differences in our approach is how we define timescales. In the GPP framework, we use growth as the reference timescale, rather than reaction or diffusion, as is often done in classical models [24, 44]. We chose this approach because growth is an observable process than can be quantified, whereas the timescales of reaction (processing) and diffusion (propagation) are more difficult to directly measure. Importantly, our simulations suggest that these timescales change in space over time. The timescales of processing and propagation vs. growth range from similar timescales (more proximally) to 25 times faster timescales for processing-propagation than growth (more distally) (Fig 1B). These findings challenge the common assumption that growth is always significantly slower than reaction and diffusion, reinforcing the need to explicitly incorporate growth into patterning models. Notably, our numerical tests on simpler domains reveal that large growth rates have a stretching effect on the pattern, while patterns subjected to slow growth are prone to“be forgotten” easily and bifurcate to patterns similar to those obtained in the absence of growth (Fig. 5B, C, S2).

While this framework highlights the importance of growth, its current formulation may require further refinement. In this model we assume isotropic, homogenous growth. However, growth is generally anisotropic and inhomogeneous, which affects patterning [45, 46, 47]. Moreover, since our model is two-dimensional, it does not account for patterning along the dorsal-ventral axis, meaning that spatial interactions in the third dimension are entirely missing from our framework. Future work could integrate a more detailed understanding of growth to better align with biological reality. Growth, patterning, and cellular differentiation are inextricably linked during development [48], and our model does not yet fully capture the complexity of these interactions.

4.2 GPP and an evolutionary perspective

Limb development follows conserved patterning principles across vertebrates, yet morphological outcomes vary significantly between species. The concept of deep homology, which describes shared developmental mechanisms underlying diverse anatomical structures, suggests that common self-organizing principles shape limb formation across evolution [49]. The GPP approach provides a framework to model these shared processes by focusing on how spatial and temporal dynamics generate variability within a unified developmental model.

By focusing on *how* rather than *what* regulates limb patterning, the GPP framework enables us to investigate homologous patterning mechanisms across species with different limb structures, such as amniotes and anamniotes (Fig. 1B, 3B). Previous studies have explored developmental variations by modifying spatial and temporal cues, focusing on specific regions or assumed discrete segmentation. In contrast, GPP treats the whole limb as a continuous field. We can reproduce known changes in digit number (Fig. 1A) and, like existing studies, potentially link them to molecular regulators such as Hox genes [20]. However, the sensitivity of patterning to positional cues highlights the need for a more accurate spatial representation of these variations in the model (Fig. 3A, C). Specifically, this would involve improving how imaging data is translated into model inputs to better capture the spatial variations in PI and AER distributions, allowing for more precise predictions of patterning outcomes [50].

Beyond capturing developmental variability, our interpretation as Growth-Processing-Propagation provides a powerful tool for exploring evolutionary shifts in limb morphology. In this context, comparing the limb development of species like axolotls and mice is particularly intriguing. Their evolutionary trajectories have diverged significantly, leading to distinct growth and patterning strategies. Yet, despite these differences, they can be studied within the same framework, enabling us to identify shared principles across tetrapods. This framework could also be extended to explore evolutionary transitions. For example, as zeugopod elongation in bats [51], digit loss in tetrapods [13] or even limb regeneration properties [52] can be reexamined as a modulation of processing and propagation relative to the growth rate. One of the most striking evolutionary transitions, the fin-to-limb shift, offers a compelling test case for this model [53]. In addition to studying changes like those in the apical ectodermal ridge (AER), GPP provides a complementary perspective: could modifications in growth rate have also contributed to key structural changes? GPP serves not only as a predictive tool but also as a means to guide future experimental work, potentially revealing the molecular pathways underlying these transitions.

In summary, our study introduces the Growth-Processing-Propagation (GPP) framework as a conceptual and numerical tool to investigate how growth dynamics influence patterning in limb development. This perspective allows us to reinterpret the interplay between reaction-diffusion systems and positional information, offering a shared self-organizing mechanism for all limb segments. Beyond its developmental applications, the framework opens new avenues for exploring evolutionary transitions. Future work will extend the model to include anisotropic growth to further bridge the gap between theoretical models and biological complexity.

5 Methods

5.1 Growth

5.1.1 Theory on growth

The movement of the tissue is characterized by the trajectories of material points within the tissue. We define the initial position of a tissue element in a two-dimensional domain using the Lagrangian coordinates $\mathbf{X} = (X_1, X_2)$. The movement of a tissue element is expressed by the bijective function $\mathbf{\Gamma}$

$$\mathbf{\Gamma} : \Re^2 \longrightarrow \Re^2, \quad \mathbf{x} = \mathbf{\Gamma}(\mathbf{X}, t) = (\Gamma_1(\mathbf{X}, t), \Gamma_2(\mathbf{X}, t)), \tag{2}$$

where $\mathbf{x}$ represents the Eulerian coordinates, i.e. the configuration at time t, and $\mathbf{\Gamma}(\mathbf{X}, 0) = \mathbf{X}$ and $\mathbf{\Gamma}^{-1}(\mathbf{x}, t) = \mathbf{X}$. Because we consider the deformation of the tissue entirely due to growth, the motion of the body is expressed by the function $\mathbf{\Gamma}$. We deduce $\mathbf{\Gamma}$ using experimental data (see section 5.1.2). The

growth velocity is then

$$\mathbf{a}(\mathbf{x},t) = \frac{d\mathbf{x}}{dt} = \frac{\partial \mathbf{\Gamma}^{-1}}{\partial t}(\mathbf{x},t), \tag{3}$$

which is described according to the current configuration. We consider the function $\mathbf{a}(\mathbf{x},t)$ to be known and twice continuously differentiable. We define the scalar

$$S(\mathbf{x},t) = \nabla \cdot \mathbf{a}, \tag{4}$$

which measures the growth rate, i.e., the rate of volumetric change per unit volume.

5.1.2 Derivation of growth from experimental images

A key challenge in resolving these equations on a growing domain lies in their formulation within the current geometry coordinates $(\mathbf{x},t)$. In this work, we address this by solving the equations directly on the evolving domain Ω_x at each time point t. It requires knowledge of the growth function $\mathbf{\Gamma}$ and the growth velocity $\mathbf{a}$. Experimental data, providing the outlines of the geometry at multiple time points, are used to deduce both (Fig. 4). For the mouse case, the outline is inspired by [54], while for the axolotl, the outline was manually extracted from images using Fiji [55].

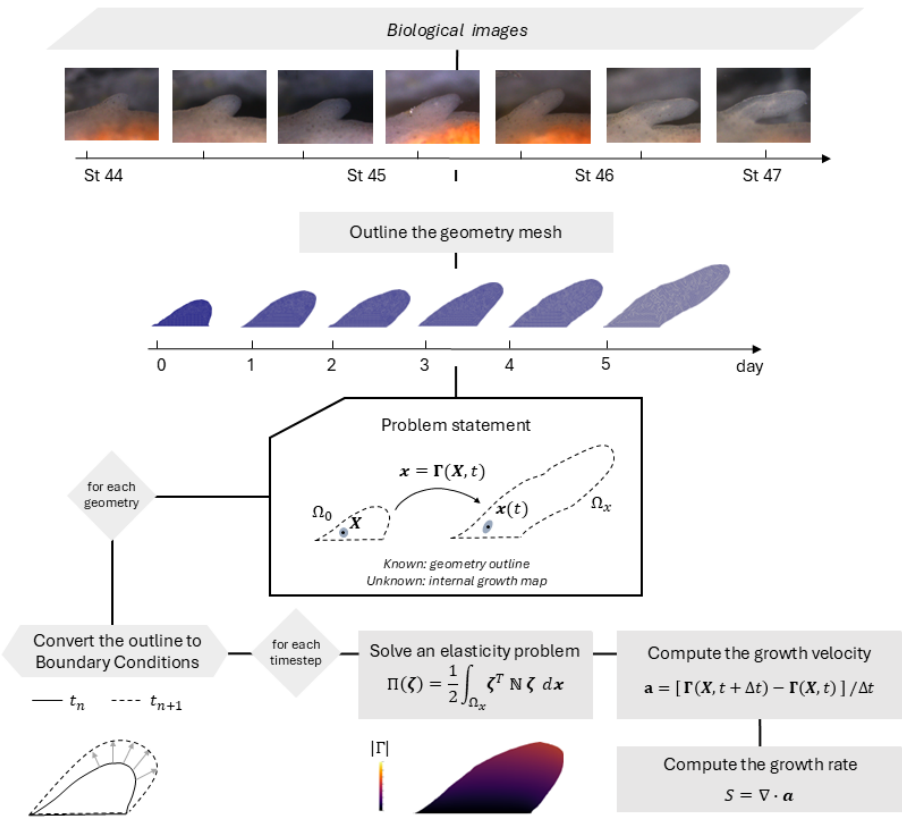

Figure 4. Numerical computation of growth rate from experimental images of developing axolotl limbs. Confocal microscopy images were taken daily for a week from the same animal. The limb outline was manually extracted from these images and meshed using triangular linear elements. The material points $\mathbf{x}(\mathbf{t})$ represent the current configuration Ω_x, which is related to their initial position $\mathbf{X}$ in Ω_0 through the mapping function $\mathbf{\Gamma}(\mathbf{X},t)$. The objective is to determine the growth map from the evolving limb geometry. Each extracted outline is converted into boundary conditions, which are enforced in an elasticity problem to solve for the displacement field ζ. This displacement is then used to compute the growth velocity $\mathbf{a}$ and the growth rate S.

Next, to compute $\mathbf{\Gamma}$, we use the minimization of a quadratic elastic energy function $\Pi(\boldsymbol{\zeta})$ with $\boldsymbol{\zeta}$ being the displacement equal to $\boldsymbol{\zeta}(t) = \mathbf{x}(t) - \mathbf{X}$,

$$\Pi(\boldsymbol{\zeta}) = \frac{1}{2}\int_{\Omega_x} \boldsymbol{\zeta}^T \, \mathbf{K} \, \boldsymbol{\zeta} \, d\mathbf{x}, \tag{5}$$

where $\mathbf{K}$ is the stiffness matrix. We assume a constant, homogeneous, and isotropic material distribution. The growth function is computed by discretizing the domain using the Finite Element Method (FEM) [56] and constraining the the displacements of the boundary nodes to match the experimental outlines.

We have as many geometries as the number of time steps. To obtain the outline for each time step, the geometry is linearly interpolated between experimental data points (Fig 4). Then, we minimize $\Pi(\boldsymbol{\zeta})$ for each time step to deduce growth displacement, $\boldsymbol{\zeta}(t)$, which can be related to the growth velocity as

$$\mathbf{a}(\mathbf{x}, t) = \frac{\boldsymbol{\zeta}(t) - \boldsymbol{\zeta}(t - \Delta t)}{\Delta t}, \tag{6}$$

where $\boldsymbol{\zeta}(t - \Delta t)$ is the displacement of the previous time step, and Δt is the size of the time step. Because we chose to linearly interpolate the growth in time, Ω_x is defined for each time step, which leads to formulate our governing equation in Eulerian coordinates.

5.2 Reaction-diffusion equation on growing domain

The reaction-diffusion equation in a growing domain is

$$\frac{d\mathbf{c}}{dt} + S(\mathbf{x}, t)\, \mathbf{c} = \mathbb{D}\, \nabla^2_{\Omega_x} \mathbf{c} + \mathbf{R}(\mathbf{c}, \mathbf{x}, t), \tag{7}$$

where $\mathbf{c}$ is the vector containing the concentrations c_i of each species ξ_i, $\mathbb{D}$ is the diffusivity matrix, and $\mathbf{R}$ is the vector of reaction terms for each species. For more details on the governing equation, please refer to Supplement S1.1. Because there is no cross-diffusion among the species, $\mathbb{D}$ is a diagonal matrix with the diffusion coefficient D_i for each species ξ_i on the diagonal.

5.2.1 Non-dimentionalization

Definition of the timescales

For simplicity, the equations are presented for a single species, but they represent a coupled system that governs the behavior of multiple species. The process of non-dimensionalization captures the interactions and interdependencies within the system.

To non-dimensionalize the system, we define $\bar{c}_i = c_i/C_i$ and $\bar{\mathbf{x}} = \mathbf{x}/L$, where C_i is a reference concentration for the ith chemical species and L is a characteristic length, which we choose to be the initial length L_0. The reaction rate ω, characteristic of the kinetic scheme, is used to non-dimensionalize the reaction term $\bar{R}(\bar{c})$. The diffusivity of the chemical species ξ_i is denoted as D_i, and we define $D_1 = \max\{D_i\}$. The non-dimensionalized diffusivity is introduced as $\bar{D}_i = D_i/D_1$.

We introduce two timescales corresponding to the two elements of eq (7), T_D and T_R for diffusivity and kinetics, respectively:

$$T_D = \frac{L_0^2}{D_1}\ , \quad T_R = \frac{1}{\omega}. \tag{8}$$

Here the characteristic timescale T_D represents the time it takes for diffusion to spread across a distance equal to the characteristic length scale L_0. The timescale T_R refers to the duration of a chemical reaction. It is typically measured as the time it takes for a change in the concentration of reactants to occur.

We define the characteristic timescale T_G, which is associated with domain expansion due to growth, as

$$T_G = \frac{L_0}{a_{ref}}, \tag{9}$$

where the reference growth velocity

$$a_{ref} = \frac{L_f - L_0}{t_f} \tag{10}$$

has been introduced. Here, t_f corresponds to the final time, at which the domain reaches the final length L_f. Rewriting the growth timescale in terms of the final strain $\varepsilon_f = \frac{L_f - L_0}{L_0}$ and using the relation $a_{ref} = \varepsilon_f L_0/t_f$, results in $T_G = t_f/\varepsilon_f$, which provides an alternative interpretation for T_G as the time required to achieve a specific strain in the domain.

Time non-dimentionalization

Any of the three timescales, T_G, T_R or T_D, could be used to non-dimensionalize the time variable. Because the growth rate is the only experimentally measurable quantity in our problem, we use it to non-dimensionalize the time variable. Taking $\tau = t/T_G$ and using (7), we obtain

$$\frac{\partial \bar{c}}{\partial \tau} + \nabla_{\bar{\Omega}_{\bar{x}}} \bar{c} \cdot \bar{\mathbf{a}} + \bar{c}\, \bar{S} = \frac{T_G}{T_D} \bar{D} \nabla^2_{\bar{\Omega}_{\bar{x}}} \bar{c} + \frac{T_G}{T_R} \bar{R}(\bar{c}, \bar{\mathbf{x}}, \tau), \tag{11}$$

dropping the bars and reverting τ back to a non-dimensional t to simplify notation, we finally have

$$\frac{\partial c}{\partial t} + \nabla_{\Omega_x} c \cdot \mathbf{a} + c\, S = \beta_D D \nabla^2_{\Omega_x} c + \alpha_R R(c, \mathbf{x}, t), \tag{12}$$

where the parameters β_D and α_R,

$$\beta_D = \frac{T_G}{T_D} = \frac{D_1 T_G}{L^2} \quad \text{and} \quad \alpha_R = \frac{T_G}{T_R} = T_G\, \omega, \tag{13}$$

have been introduced.

One of the advantages of this approach lies in the explicit knowledge of T_G, which facilitates the conversion of non-dimensionalized results back into the dimensionalized form.

Interpretation of the parameters α_R and β_D

The parameters α_R and β_D represent the relative timescales of growth with respect to reaction and diffusion, respectively (Fig. 5A). These parameters provide an intuitive framework for interpreting the system's dynamics. When both parameters change simultaneously, it indicates that the rate of growth is varying. Values of α_R and β_D less than 1 signify that the rate of growth exceeds the reaction-diffusion timescale, causing growth rate to outpace the formation of patterns (Fig. 5B). When these parameters equal 1, all processes proceed at the same rate. For values greater than 1, the reaction-diffusion processes dominate over growth rate, leading to results similar to those obtained for a static (non-growing) system (Fig. 5C).

5.3 Numerical Simulations

The governing equation (7) was discretized in space using the Finite Element Method and in time with the implicit midpoint rule. The numerical implementation was performed in MATLAB [57]. Linear triangular elements with four-point Gauss quadrature where used to mesh the domain. The number of time increments was given by $\varepsilon_f/\Delta t$, with Δt the time step. Homogeneous Neumann boundary conditions were applied. The function $\mathbf{R}$ follows Schnakenberg kinetics [58] with model parameters a, b, and d that ensure pattern formation (see supplement S2.2 for details).

Simulations were initialized with random perturbations (10% variation) around the steady state defined by $\mathbf{R}(\mathbf{c}) = \mathbf{0}$. For mice and axolotl limb models, an epithelial layer was included at $t = 0$ with $\mathbf{c}(0) = \mathbf{0}$ (Fig. 1, 2, 3). The effect of this initial condition is further explored in Fig. S3.

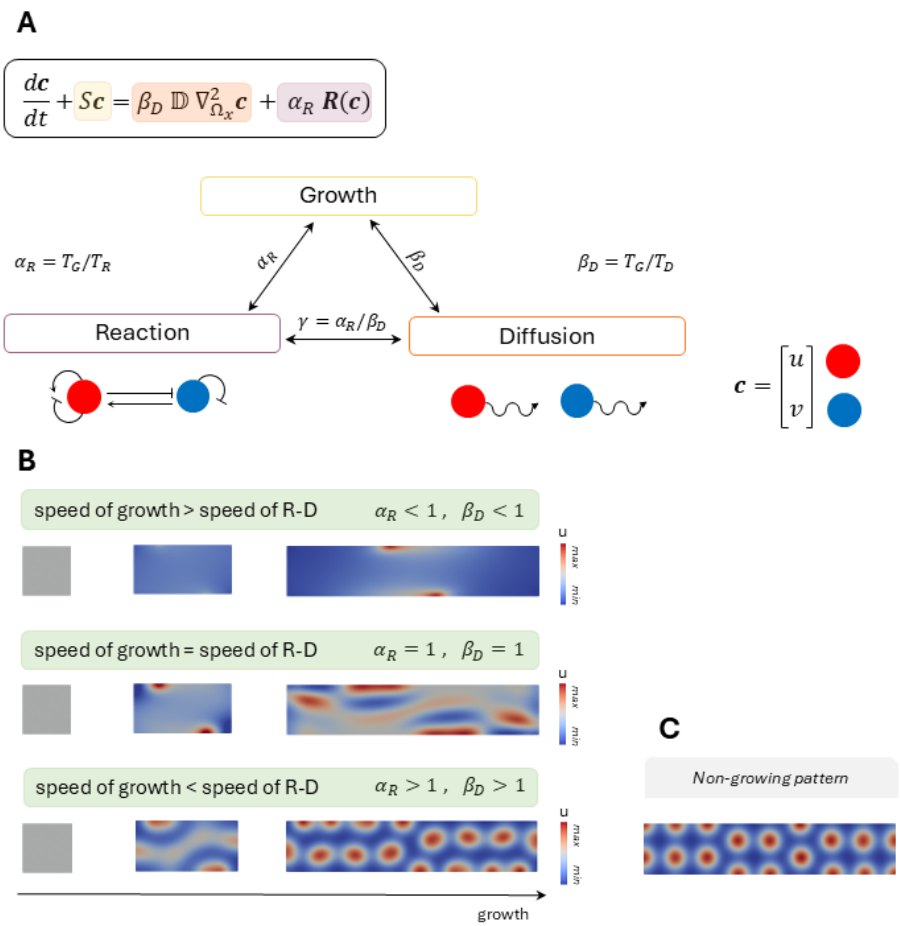

Figure 5. Growth-Reaction-Diffusion System. (**A**) Schematic representation of the Reaction-Diffusion system with growth, mathematically equivalent to the GPP model but without its biological interpretation. (**B**) Simulated patterns on a growing rectangle for varying α_R and β_D. Results for an initial, intermediate and final domain size are shown. (**C**) Comparison with a non-growing rectangle ($\alpha_R > 1$, $\beta_D > 1$)

References

[1] Cheryll Tickle. The number of polarizing region cells required to specify additional digits in the developing chick wing. *Nature*, 289(5795):295–298, 1981.

[2] Randy L Johnson and Clifford J Tabin. Molecular models for vertebrate limb development. *Cell*, 90(6):979–990, 1997.

[3] Francesca V Mariani, Christina P Ahn, and Gail R Martin. Genetic evidence that fgfs have an instructive role in limb proximal–distal patterning. *Nature*, 453(7193):401–405, 2008.

[4] Lewis Wolpert. Positional information and the spatial pattern of cellular differentiation. *Journal of theoretical biology*, 25(1):1–47, 1969.

[5] Rolf Zeller, Javier Lopez-Rios, and Aimee Zuniga. Vertebrate limb bud development: Moving towards integrative analysis of organogenesis. *Nature Reviews Genetics*, 10(12):845–858, 2009.

[6] Paul J Scherz, Brian D Harfe, Andrew P McMahon, and Clifford J Tabin. The limb bud shh-fgf feedback loop is terminated by expansion of former zpa cells. *Science*, 305(5682):396–399, 2004.

[7] Jozsef Zakany and Denis Duboule. The role of hox genes during vertebrate limb development. *Current opinion in genetics & development*, 17(4):359–366, 2007.

[8] Robert D Riddle, Randy L Johnson, Ed Laufer, and Cliff Tabin. Sonic hedgehog mediates the polarizing activity of the zpa. *Cell*, 75(7):1401–1416, 1993.

[9] John W Saunders Jr. The proximo-distal sequence of origin of the parts of the chick wing and the role of the ectoderm. *Journal of Experimental Zoology*, 108(3):363–403, 1948.

[10] Alberto Roselló-Díez, María A Ros, and Miguel Torres. Diffusible signals, not autonomous mechanisms, determine the main proximodistal limb subdivision. *Science*, 332(6033):1086–1088, 2011.

[11] Kimberly L Cooper, Jimmy Kuang-Hsien Hu, Derk ten Berge, Marian Fernandez-Teran, Maria A Ros, and Clifford J Tabin. Initiation of proximal-distal patterning in the vertebrate limb by signals and growth. *Science*, 332(6033):1083–1086, 2011.

[12] Nadia Mercader, Esther Leonardo, María Elisa Piedra, Carlos Martínez-A, María Ángeles Ros, and Miguel Torres. Opposing ra and fgf signals control proximodistal vertebrate limb development through regulation of meis genes. *Development*, 127(18):3961–3970, 2000.

[13] Aditya Saxena, Matthew Towers, and Kimberly L Cooper. The origins, scaling and loss of tetrapod digits. *Philosophical Transactions of the Royal Society B: Biological Sciences*, 372(1713):20150482, 2017.

[14] Alan Mathison Turing. The chemical basis of morphogenesis. *Bulletin of mathematical biology*, 52:153–197, 1990.

[15] Luciano Marcon and James Sharpe. Turing patterns in development: What about the horse part? *Current Opinion in Genetics & Development*, 22(6):578–584, 2012.

[16] Jelena Raspopovic, Luciano Marcon, Laura Russo, and James Sharpe. Digit patterning is controlled by a bmp-sox9-wnt turing network modulated by morphogen gradients. *Science*, 345(6196):566–570, 2014.

[17] Jianjian Zhu, Eiichiro Nakamura, Minh-Thanh Nguyen, Xiaozhong Bao, Haruhiko Akiyama, and Susan Mackem. Uncoupling Sonic Hedgehog Control of Pattern and Expansion of the Developing Limb Bud. *Developmental Cell*, 14(4):624–632, 2008.

[18] Jianjian Zhu, Rashmi Patel, Anna Trofka, Brian D. Harfe, and Susan Mackem. Sonic hedgehog is not a limb morphogen but acts as a trigger to specify all digits in mice. *Developmental Cell*, 57(17):2048–2062.e4, 2022.

[19] Kristina S. Stapornwongkul and Jean-Paul Vincent. Generation of extracellular morphogen gradients: The case for diffusion. *Nature Reviews Genetics*, 22(6):393–411, 2021.

[20] Rushikesh Sheth, Luciano Marcon, M Félix Bastida, Marisa Junco, Laura Quintana, Randall Dahn, Marie Kmita, James Sharpe, and Maria A Ros. Hox genes regulate digit patterning by controlling the wavelength of a turing-type mechanism. *Science*, 338(6113):1476–1480, 2012.

[21] Amarendra Badugu, Conradin Kraemer, Philipp Germann, Denis Menshykau, and Dagmar Iber. Digit patterning during limb development as a result of the bmp-receptor interaction. *Scientific reports*, 2(1):991, 2012.

[22] Takashi Miura, Kohei Shiota, Gillian Morriss-Kay, and Philip K Maini. Mixed-mode pattern in doublefoot mutant mouse limbâturing reaction–diffusion model on a growing domain during limb development. *Journal of Theoretical Biology*, 240(4):562–573, 2006.

[23] Soha Ben Tahar, Jose J Muñoz, Sandra J Shefelbine, and Ester Comellas. Turing pattern prediction in three-dimensional domains: the role of initial conditions and growth. *bioRxiv*, pages 2023–03, 2023.

[24] Edmund John Crampin. *Reaction-diffusion patterns on growing domains.* PhD thesis, University of Oxford, 2000.

[25] Edmund J Crampin, Eamonn A Gaffney, and Philip K Maini. Reaction and diffusion on growing domains: scenarios for robust pattern formation. *Bulletin of mathematical biology*, 61(6):1093–1120, 1999.

[26] Ramón G Plaza, Faustino Sanchez-Garduno, Pablo Padilla, Rafael A Barrio, and Philip K Maini. The effect of growth and curvature on pattern formation. *Journal of dynamics and differential equations*, 16:1093–1121, 2004.

[27] Philip K Maini, Thomas E Woolley, Ruth E Baker, Eamonn A Gaffney, and S Seirin Lee. Turing's model for biological pattern formation and the robustness problem. *Interface focus*, 2(4):487–496, 2012.

[28] Andrew L Krause, Meredith A Ellis, and Robert A Van Gorder. Influence of curvature, growth, and anisotropy on the evolution of turing patterns on growing manifolds. *Bulletin of mathematical biology*, 81:759–799, 2019.

[29] Dennis Summerbell. Interaction between the proximo-distal and antero-posterior co-ordinates of positional value during the specification of positional information in the early development of the chick limb-bud. *Development*, 32(1):227–237, 1974.

[30] Anna M Raines, Bliss Magella, Mike Adam, and S Steven Potter. Key pathways regulated by hoxa9, 10, 11/hoxd9, 10, 11 during limb development. *BMC developmental biology*, 15:1–15, 2015.

[31] Nadia B Fröbisch and Neil H Shubin. Salamander limb development: integrating genes, morphology, and fossils. *Developmental Dynamics*, 240(5):1087–1099, 2011.

[32] David M Gardiner, Bruce Blumberg, Yuriko Komine, and Susan V Bryant. Regulation of hoxa expression in developing and regenerating axolotl limbs. *Development*, 121(6):1731–1741, 1995.

[33] Maureen A Torok, David M Gardiner, Juan-Carlos Izpisúa-Belmonte, and Susan V Bryant. Sonic hedgehog (shh) expression in developing and regenerating axolotl limbs. *Journal of Experimental Zoology*, 284(2):197–206, 1999.

[34] Jixing Zhong, Rita Aires, Georgios Tsissios, Evangelia Skoufa, Kerstin Brandt, Tatiana Sandoval-Guzmán, and Can Aztekin. Multi-species atlas resolves an axolotl limb development and regeneration paradox. *Nature Communications*, 14(1):6346, 2023.

[35] Eugeniu Nacu, Elena Gromberg, Catarina R Oliveira, David Drechsel, and Elly M Tanaka. Fgf8 and shh substitute for anterior–posterior tissue interactions to induce limb regeneration. *Nature*, 533(7603):407–410, 2016.

[36] Giacomo L Glotzer, Pietro Tardivo, and Elly M Tanaka. Canonical wnt signaling and the regulation of divergent mesenchymal fgf8 expression in axolotl limb development and regeneration. *Elife*, 11:e79762, 2022.

[37] Sruthi Purushothaman, Ahmed Elewa, and Ashley W Seifert. Fgf-signaling is compartmentalized within the mesenchyme and controls proliferation during salamander limb development. *Elife*, 8:e48507, 2019.

[38] Yiping Chen and Xiang Zhao. Shaping limbs by apoptosis. *Journal of Experimental Zoology*, 282(6):691–702, 1998.

[39] Etienne Vincent, Eric Villiard, Fadi Sader, Sabin Dhakal, Benjamin H Kwok, and Stéphane Roy. Bmp signaling is essential for sustaining proximo-distal progression in regenerating axolotl limbs. *Development*, 147(14):dev170829, 2020.

[40] Kathleen Roensch, Akira Tazaki, Osvaldo Chara, and Elly M Tanaka. Progressive specification rather than intercalation of segments during limb regeneration. *Science*, 342(6164):1375–1379, 2013.

[41] Lewis S Mosby, Amy E Bowen, and Zena Hadjivasiliou. Morphogens in the evolution of size, shape and patterning. *Development*, 151(18):dev202412, 2024.

[42] Tom W Hiscock, Patrick Tschopp, and Clifford J Tabin. On the formation of digits and joints during limb development. *Developmental cell*, 41(5):459–465, 2017.

[43] Shigeru Kondo and Takashi Miura. Reaction-diffusion model as a framework for understanding biological pattern formation. *Science*, 329(5999):1616–1620, 2010.

[44] James Dickson Murray. Spatial models and biomedical applications. *Mathematical Biology*, 2003.

[45] Bernd Boehm, Henrik Westerberg, Gaja Lesnicar-Pucko, Sahdia Raja, Michael Rautschka, James Cotterell, Jim Swoger, and James Sharpe. The role of spatially controlled cell proliferation in limb bud morphogenesis. *PLoS biology*, 8(7):e1000420, 2010.

[46] Yoshihiro Morishita and Takayuki Suzuki. Bayesian inference of whole-organ deformation dynamics from limited space-time point data. *Journal of theoretical biology*, 357:74–85, 2014.

[47] Gaja Lesnicar-Pucko, Julio M Belmonte, Marco Musy, James A Glazier, and James Sharpe. Cellular mechanisms of chick limb bud morphogenesis. *bioRxiv*, pages 2020–09, 2020.

[48] Helms Jill A. Nusse Roel Derk ten Berge, Brugmann Samantha A. Wnt and fgf signals interact to coordinate growth with cell fate specification during limb development. *Development*, 135(19):3247–3257, 2008.

[49] Neil Shubin, Cliff Tabin, and Sean Carroll. Deep homology and the origins of evolutionary novelty. *Nature*, 457(7231):818–823, 2009.

[50] Laura Aviñó-Esteban, Heura Cardona-Blaya, and James Sharpe. Spatio-temporal reconstruction of gene expression patterns in developing mice. *Development*, 152(4), 2025.

[51] Karen E Sears, Richard R Behringer, John J Rasweiler IV, and Lee A Niswander. Development of bat flight: morphologic and molecular evolution of bat wing digits. *Proceedings of the National Academy of Sciences*, 103(17):6581–6586, 2006.

[52] Sylvain Darnet, Aline C Dragalzew, Danielson B Amaral, Josane F Sousa, Andrew W Thompson, Amanda N Cass, Jamily Lorena, Eder S Pires, Carinne M Costa, Marcos P Sousa, et al. Deep evolutionary origin of limb and fin regeneration. *Proceedings of the National Academy of Sciences*, 116(30):15106–15115, 2019.

[53] Koh Onimaru, Luciano Marcon, Marco Musy, Mikiko Tanaka, and James Sharpe. The fin-to-limb transition as the re-organization of a turing pattern. *Nature Communications*, 7(1):11582, 2016.

[54] Marco Musy, Kevin Flaherty, Jelena Raspopovic, Alexandre Robert-Moreno, Joan T Richtsmeier, and James Sharpe. A quantitative method for staging mouse embryos based on limb morphometry. *Development*, 145(7):dev154856, 2018.

[55] Johannes Schindelin, Ignacio Arganda-Carreras, Erwin Frise, Verena Kaynig, Mark Longair, Tobias Pietzsch, Stephan Preibisch, Curtis Rueden, Stephan Saalfeld, Benjamin Schmid, et al. Fiji: an open-source platform for biological-image analysis. *Nature methods*, 9(7):676–682, 2012.

[56] Olgierd Cecil Zienkiewicz and Robert Leroy Taylor. *The finite element method for solid and structural mechanics*. Elsevier, 2005.

[57] The MathWorks, Inc. *MATLAB version R2023a*. The MathWorks, Inc., Natick, Massachusetts, 2023. Available at `https://www.mathworks.com/products/matlab.html`.

[58] Jürgen Schnakenberg. Simple chemical reaction systems with limit cycle behaviour. *Journal of theoretical biology*, 81(3):389–400, 1979.

Supplementary Information

S0 Supplementary figures & tables

S1.1 Table: Parameter selection for patterning simulations

	Turing Space			α							β		
Parameters	a	b	d	α_R	α_{R1}	l_1	a_1	α_{R2}	l_2	a_2	β_D	β_{D1}	N
Mice	0.47	2	113	1	2	0.13	0.03	8	0.45	0.03	1	26	30
Axolotl	0.47	2	113	1	5	0.25	0.05	35	0.75	0.05	1	15	12

Table S1. Parameter values used for different cases. The parameters a and b correspond to the kinetic terms of the Schnakenberg system, as described in Eq. (S.11) [58]. The relative diffusion of v with respect to u (d) is seen in Eq. (S.10). The parameters α_R, $\alpha_R 1$, and $\alpha_R 2$ represent the values of positional information shown in Fig. 1B and Fig. 3B. The parameters l_1 and l_2 define the transition positions between the stylopod and zeugopod, and between the zeugopod and autopod regions, respectively, relative to the final limb length. The parameters a_1 and a_2 control the smoothness of these transitions. The parameters β_D and β_{D1} indicate the AER values shown in Fig. 1B and Fig. 3B. Finally, N represents the number of elements used to define the thickness of the AER. AER parameters are explored in SUPP. S4.

For Fig. 5, the Turing space parameters are the same as those used for mice and axolotl. The values for α_R and β_D were set to 0.1 for low values and 10 for high values.

S2.2 Figures

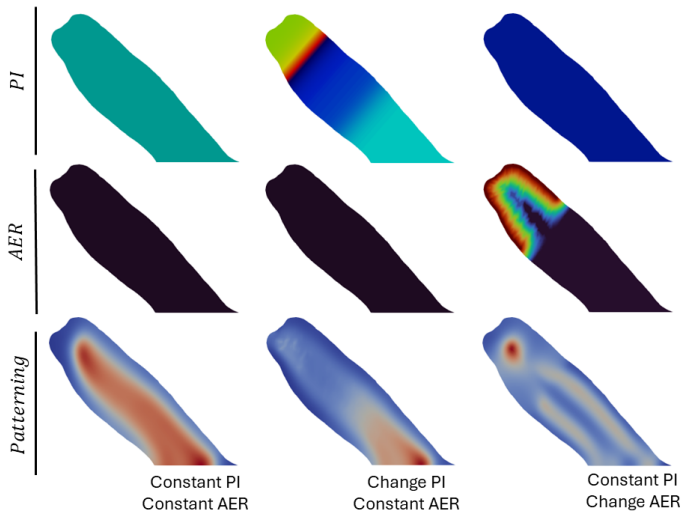

Figure S1. Effect of the AER and PI on the axolotl limb. The first column represents the framework without incorporating positional information (PI) or the apical ectodermal ridge (AER), resulting in a simple stripe pattern. The second column includes PI but excludes AER, maintaining the proximal pattern while losing the autopod pattern. The third column incorporates AER but excludes PI, where PI takes a homogeneous value corresponding to the zeugopod. As a result, the patterning leads to an extended zeugopod-like element.

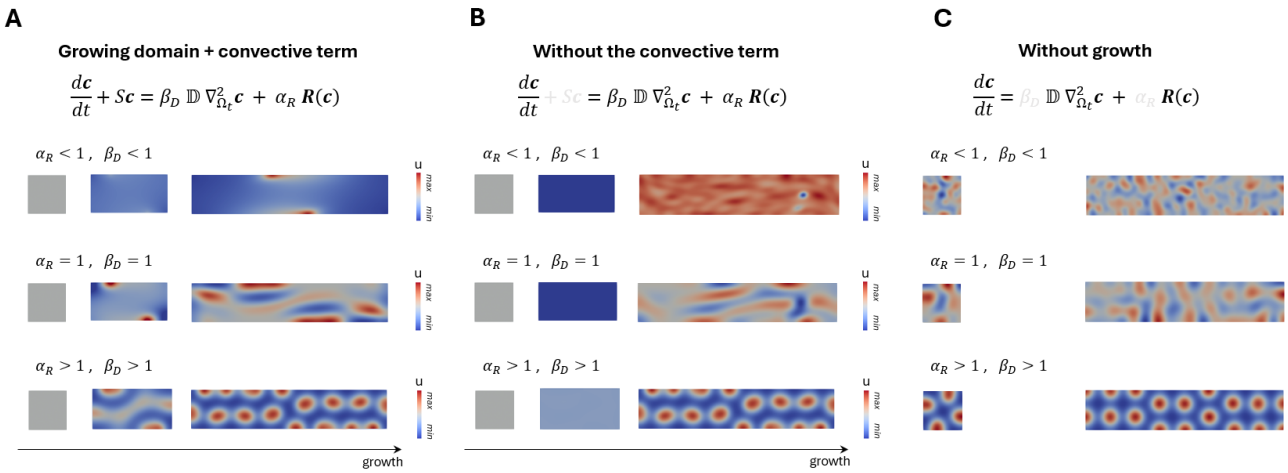

Figure S2. Effect of the convective term on pattern formation in growing domains. (A) Simulation on a growing rectangular domain including the convective term, as described in the main text. **(B)** Simulation on a growing domain without the convective term. Lower values of α_R and β_D show a noticeable impact of the convective term on the resulting pattern. **(C)** Simulation on a static domain (no growth), where the convective term is absent by definition. In this case, α_R and β_D lose their influence on the pattern's shape, and all simulations yield the same final pattern. Higher values of α_R and β_D only accelerate the convergence of the pattern.

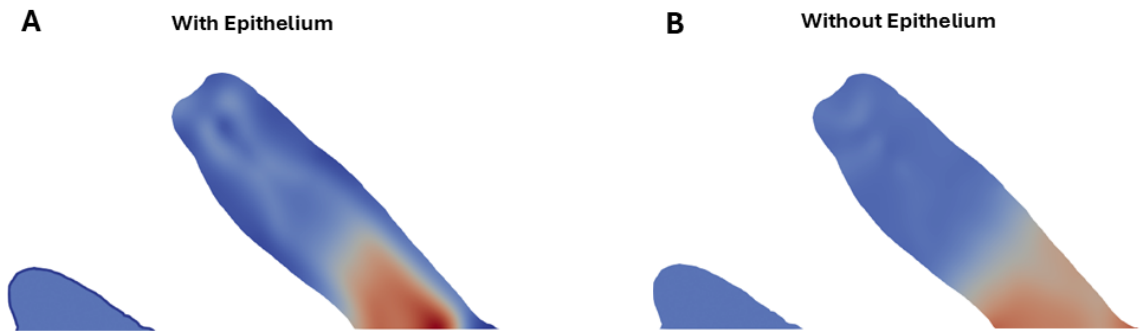

Figure S3. Effect of the epithelium on pattern formation. (**A**) Pattern formation with an epithelium boundary condition. The epithelium is modeled by setting $u(0) = 0$ and $v(0) = 0$ in the first two layers of elements. The rest of the elements are initialized at the steady-state solution (u_0, v_0), defined as $\mathbf{R}(u_0, v_0) = \mathbf{0}$. (**B**) Pattern formation without the epithelium. All elements are initialized at the steady-state solution (u_0, v_0). Both cases have different initial conditions at $t = 0$, without any additional specification on the epithelium for $t > 0$.

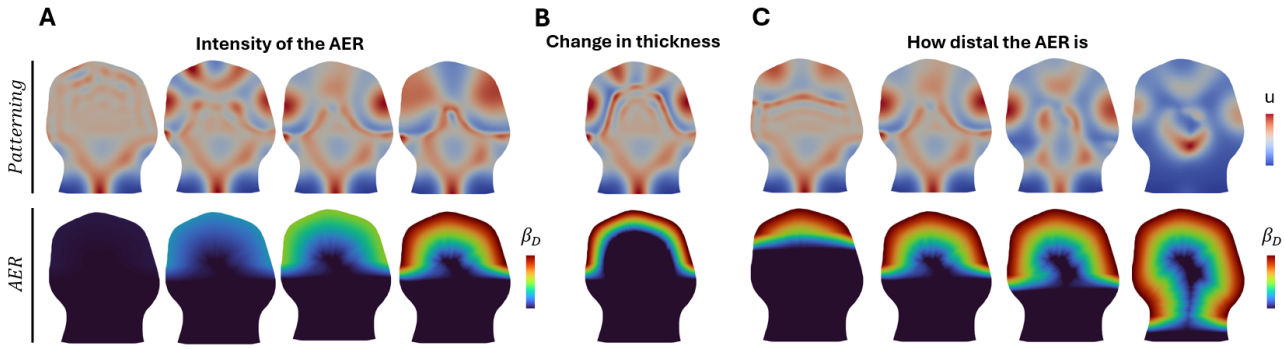

Figure S4. Influence of AER properties on limb bud patterning. (**A**) The intensity of the AER, (**B**) Change in AER thickness, and (**C**) the proximodistal positioning of the AER influence patterning within the limb bud. The top row shows the resulting patterning in the limb, while the bottom row shows the corresponding AER. Color scales indicate the spatial variations in patterning (top row, u) and AER properties (bottom row, β_D).

S0 Turing space through linear stability analysis

This appendix presents the derivation of the equations governing the Growth-Processing-Propagation system and describes the linear stability analysis used to identify the range of parameters that ensure pattern

formation.

S1.1 Derivation of the reaction-diffusion equation in a growing domain

We consider a growing domain Ω_x enclosed by a surface $\partial\Omega_x$. From the general conservation equation, the amount of material in Ω_x is equal to the rate of growth velocity of this material across $\partial\Omega_x$ into Ω_x, plus the material created in Ω_x. For a species ξ with a concentration c, this can be expressed by

$$\frac{d}{dt}\int_{\Omega_x} c(\mathbf{x},t)d\mathbf{x} = -\int_{\partial\Omega_x} \mathbf{j}\cdot\mathbf{ds} + \int_{\Omega_x} R\, d\mathbf{x}, \tag{S.1}$$

where $\mathbf{j}$ is the flux of material going through $\mathbf{ds} = \mathbf{n}\, ds$ with $\mathbf{n}$ the normal of the surface element ds. The source of material is R, which can depend on the vector of morphogens concentration c, the position vector $\mathbf{x}$, and the time t. By applying the divergence theorem to the surface integral, the previous equation becomes

$$\frac{d}{dt}\int_{\Omega_x} c(\mathbf{x},t)d\mathbf{x} = \int_{\Omega_x} \left[-\nabla\cdot\mathbf{j} + R(c,\mathbf{x},t)\right] d\mathbf{x}. \tag{S.2}$$

In order to evaluate the left-hand term, we use the Reynolds transport theorem

$$\frac{d}{dt}\int_{\Omega_x} c(\mathbf{x},t)d\mathbf{x} = \int_{\Omega_x} \left[\frac{\partial c}{\partial t} + \nabla\cdot(\mathbf{a}c)\right] d\mathbf{x}, \tag{S.3}$$

where $\mathbf{a}(\mathbf{x},t)$ is the growth velocity, and the evolution equation becomes

$$\int_{\Omega_x} \left[\frac{\partial c}{\partial t} + \nabla\cdot\mathbf{a}c\right] d\mathbf{x} = \int_{\Omega_x} \left[-\nabla\cdot\mathbf{j} + R(c,\mathbf{x},t)\right] d\mathbf{x}. \tag{S.4}$$

As this must hold true for any t, the integrands must be equal to each other. Therefore, we obtain the *local conservation equation* for c which is

$$\frac{\partial c}{\partial t} + \nabla_{\Omega_x}\cdot(\mathbf{a}c) = -\nabla_{\Omega_x}\cdot\mathbf{j} + R(c,\mathbf{x},t). \tag{S.5}$$

Here, $\mathbf{j}$ is a general flux transport vector, which can be diffusion or another process. We consider a classical diffusion problem,

$$\mathbf{j} = -D\nabla_{\Omega_x} c, \tag{S.6}$$

where D is the diffusivity at constant density. Equation (S.5) becomes

$$\frac{\partial c}{\partial t} + \nabla_{\Omega_x}\cdot(\mathbf{a}c) = \nabla_{\Omega_x}\cdot(D\nabla_{\Omega_x} c) + R(c,\mathbf{x},t), \tag{S.7}$$

where D may be a function of $\mathbf{x}$ and c. The time-varying domain introduces two terms: $\nabla c\cdot\mathbf{a}$ and $c\,\nabla\cdot\mathbf{a}$. The first represents the transport of material around the domain at a certain rate (dependent of the growth velocity $\mathbf{a}$), in other terms it corresponds to the elemental volume moving with the growth velocity. The second one represents the dilution effect due to the local volume increase. The equation becomes

$$\frac{\partial c}{\partial t} + \nabla_{\Omega_x} c\cdot\mathbf{a} + c\,\nabla_{\Omega_x}\cdot\mathbf{a} = D\nabla^2_{\Omega_x} c + R(c,\mathbf{x},t), \tag{S.8}$$

where D has been assumed to be independent of the spatial variable $\mathbf{x}$. Taking into account (4), the final equation is

$$\frac{dc}{dt} + S(\mathbf{x},t)\, c = D\nabla^2_{\Omega_x} c + R(c,\mathbf{x},t), \tag{S.9}$$

where $S(\mathbf{x},t)$ is the growth rate.

S2.2 Linear Stability Analysis in a growing domain

We perform a linear stability analysis to determine the Turing space of parameters in a growing domain. First, we deduce the form of growth that yields a constant growth rate S in the linearized system. Then, we analyze its stability both with and without diffusion [44]. For pattern formation to occur, the system must be stable without diffusion and unstable with diffusion. These conditions yield four equations that define the set of parameters capable of generating patterns.

To derive the following system of two equations, we rearrange (12). The linear stability analysis is then performed on a two-species system with $\mathbf{c} = (u, v)$,

$$\begin{aligned} \frac{du}{dt} =& \beta_D \nabla^2_{\Omega_x} u + \alpha_R f(u,v) - uS(\mathbf{x},t), \\ \frac{dv}{dt} =& \beta_D d \nabla^2_{\Omega_x} v + \alpha_R g(u,v) - vS(\mathbf{x},t), \end{aligned} \tag{S.10}$$

where $f(u, v)$ and $g(u, v)$ are the reaction terms for species u and v, respectively. The form of the functions follow the Schnakenberg kinetics

$$\begin{aligned} f(u,v) &= a - u + u^2 v, \\ g(u,v) &= b - u^2 v, \end{aligned} \tag{S.11}$$

from [58]. The ratio of their diffusivities is given by $d = D_v/D_u$. The parameters α_R and β_D are non-dimensional quantities as defined in (13). Our objective is to identify a homogeneous steady state that remains stable under small perturbations in the absence of diffusion, but becomes unstable when small spatial perturbations are introduced in the presence of diffusion.

The homogeneous steady state is defined as the solution of the system (S.10) with both time and space independence. This solution can only be found if we assume that $S(\mathbf{x}, t)$ is a constant S. The homogeneous steady state can be determined by solving the following equations,

$$\alpha_R f(u_0, v_0) - u_0 S = 0 \quad \text{and} \quad \alpha_R g(u_0, v_0) - v_0 S = 0. \tag{S.12}$$

Introducing a small perturbation to the homogeneous steady state,

$$\begin{aligned} u &= u_0 + w_1(\mathbf{x}, t), \\ v &= v_0 + w_2(\mathbf{x}, t), \end{aligned} \tag{S.13}$$

and substituting it into (S.10), the linearized system

$$\begin{bmatrix} w_{1t} \\ w_{2t} \end{bmatrix} = \alpha_R \begin{bmatrix} f_u & f_v \\ g_u & g_v \end{bmatrix}_{(u_0,v_0)} \begin{bmatrix} w_1 \\ w_2 \end{bmatrix} + \beta_D \begin{bmatrix} 1 & 0 \\ 0 & d \end{bmatrix} \nabla^2_{\Omega_x} \begin{bmatrix} w_1 \\ w_2 \end{bmatrix} - S \begin{bmatrix} w_1 \\ w_2 \end{bmatrix} \tag{S.14}$$

is obtained, where the subindex indicates a time derivative, and $\mathbb{A}$ is the Jacobian matrix of f and g evaluated at (u_0, v_0),

$$\mathbb{A} = \begin{bmatrix} f_u & f_v \\ g_u & g_v \end{bmatrix}_{(u_0,v_0)}, \quad \text{and} \quad \mathbb{D} = \begin{bmatrix} 1 & 0 \\ 0 & d \end{bmatrix}, \tag{S.15}$$

with $\mathbb{D}$ the diffusivity matrix.

Growth function for the linear analysis

To determine the linearized solution, the growth rate $S(\mathbf{x}, t)$ must constant in both time and space. The goal is to identify a growth function $\mathbf{x}(t) = \mathbf{\Gamma}(\mathbf{X}, t)$ that yields a constant S. For simplicity, the analysis is restricted to one dimension.

An exponential growth function is first considered:

$$x = X\, \mathrm{e}^{\kappa t}, \tag{S.16}$$

with growth velocity

$$a = \frac{\partial \Gamma}{\partial t} = \kappa X \, \mathrm{e}^{\kappa t} = \kappa x, \tag{S.17}$$

leading to a constant growth rate:

$$S = \frac{\partial a}{\partial x} = \kappa. \tag{S.18}$$

This exponential form maintains a constant $S(x,t)$, satisfying the requirements for the linear stability analysis.

For comparison, a linear growth function is also examined:

$$x = X + X\kappa t \Longrightarrow X = \frac{x}{1+\kappa t}, \tag{S.19}$$

where κ is a known scalar. The corresponding growth velocity is

$$a(x,t) = \frac{\partial \Gamma}{\partial t} = \kappa X = \kappa \, \frac{x}{1+\kappa t}, \tag{S.20}$$

yielding a time-dependent growth rate:

$$S(x,t) = \frac{\partial a}{\partial x} = \frac{\kappa}{1+\kappa t}. \tag{S.21}$$

In this case, $S(\mathbf{x},t)$ is unsuitable for the linearization.

Linearized solution

We assume a general form for the solution to (S.10)

$$\begin{bmatrix} w_1(\mathbf{x},t) \\ w_2(\mathbf{x},t) \end{bmatrix} = \exp(\lambda t) \begin{bmatrix} \Phi_1(\mathbf{x}) \\ \Phi_2(\mathbf{x}) \end{bmatrix}, \tag{S.22}$$

where λ is an eigenvalue of $\alpha_R \mathbb{A}$, and $\Phi_{1,2}(\mathbf{x})$ are the components of the eigenvector of the spatial problem. Substituting this into the linearized equation (S.14) yields

$$\beta_D \mathbb{D} \nabla^2 \mathbf{\Phi} + [\alpha_R \mathbb{A} - [\lambda + S] \, \mathbb{I} \,] \, \mathbf{\Phi} = \mathbf{0}, \tag{S.23}$$

where $\mathbb{I}$ is the 2×2 identity matrix and $\mathbf{\Phi}$ is the vector $[\Phi_1, \Phi_2]$. The solution that satisfies equation (S.23) can be expressed as $\mathbf{\Phi}_m = \mathbf{y}_m \Phi_m$, where $\mathbf{y}_m$ is a constant vector and $\Phi_m(\mathbf{x})$ is a scalar eigenfunction of the Laplacian satisfying the boundary conditions. This implies that $\nabla^2 \Phi_m(\mathbf{x}) = -k_m^2 \Phi_m(\mathbf{x})$, where k_m is the wavenumber corresponding to each Φ_m. Therefore, equation (S.23) becomes

$$[-\beta_D \mathbb{D} k_m^2 + [\alpha_R \mathbb{A} - [\lambda + S] \, \mathbb{I} \,] \, \mathbf{y}_m = \mathbf{0}, \tag{S.24}$$

For non-trivial solutions, the determinant must satisfy

$$| - \beta_D \mathbb{D} k_m^2 + [\alpha_R \mathbb{A} - [\lambda + S] \, \mathbb{I} \,]| = 0, \tag{S.25}$$

leading to the dispersion relation $\lambda = \lambda(k_m^2)$. It can be written as

$$\lambda^2 + \lambda \left[\beta_D \, [1+d] \, k_m^2 - \alpha_R \, [f_u + g_v] + 2 \, S\right] + h(k_m^2) = 0, \tag{S.26}$$

where

$$h(k_m^2) = k_m^4 \, \beta_D^2 d + k_m^2 \, \beta_D \Big[[1+d] \, S - \alpha_R \, [d \, f_u + g_v]\Big] + \Big[\alpha_R^2 [f_u \, g_v - f_v \, g_u] - \alpha_R \, [f_u + g_v] \, S + S^2\Big]. \tag{S.27}$$

Stability without diffusion

To determine the stability of the solution, we examine the sign of the real part of $\lambda(k_m^2)$. If $\mathfrak{Re}(\lambda) < 0$, the solution is stable (decreasing in time), and if $\mathfrak{Re}(\lambda) > 0$, the solution is unstable (increasing exponentially in time). Without diffusion ($k = 0$), the equation becomes

$$\lambda^2 - \lambda\,[\,\alpha_R\,[f_u + g_v] - 2\,S\,] + \alpha^2\,[f_u\,g_v - f_v\,g_u] - \alpha_R\,[f_u + g_v]\,S + S^2 = 0, \tag{S.28}$$

whose roots are

$$2\lambda_0^{\pm} = [\,\alpha_R\,[f_u + g_v] - 2\,S] \pm \sqrt{(\,\alpha_R\,[f_u + g_v] - 2\,S)^2 - 4[\alpha_R^2\,[f_u\,g_v - f_v\,g_u] - \alpha_R\,[f_u + g_v]\,S + S^2]}. \tag{S.29}$$

For λ_0^-, the condition for stability is

$$\alpha_R\,[f_u + g_v] - 2\,S < 0, \tag{S.30}$$

which can be rewritten in terms of the trace of $\mathbb{A}$ to obtain the first condition

$$\alpha_R\,tr(\mathbb{A}) - 2S < 0. \tag{S.31}$$

For λ_0^+ to be negative, we require

$$[\,\alpha_R\,[f_u + g_v] - 2\,S] > \sqrt{(\,\alpha_R\,[f_u + g_v] - 2\,S)^2 - 4[\alpha_R^2\,[f_u\,g_v - f_v\,g_u] - \alpha_R\,[f_u + g_v]\,S + S^2]}, \tag{S.32}$$

which can be written as

$$\alpha^2\,[f_u\,g_v - f_v\,g_u] - \alpha\,[f_u + g_v]\,S + S^2 > 0, \tag{S.33}$$

resulting in

$$\alpha^2\,|\mathbb{A}| - \alpha\,tr(\mathbb{A})\,S + S^2 > 0, \tag{S.34}$$

which is the second condition.

Instability with diffusion

When considering diffusion in equation (S.26), the roots are

$$2\,\lambda^{\pm}(k_m^2) = -\left[\beta_D\,[1 + d]\,k_m^2 - \alpha_R\,[f_u + g_v] + 2\,S\right] \pm \sqrt{(\beta_D\,[1 + d]\,k_m^2 - \alpha_R\,[f_u + g_v] + 2\,S)^2 - 4h(k_m^2)}, \tag{S.35}$$

Given the condition for stability (S.31), necessarily

$$\beta_D\,[1 + d]\,k_m^2 - \alpha_R\,[f_u + g_v] + 2\,S > 0, \tag{S.36}$$

and therefore, $\lambda^-(k_m^2)$ is always negative. To ensure instability, $\lambda^+(k_m^2)$ must be positive, which requires

$$h(k_m^2) < 0.$$

This leads to the condition

$$k_m^4\,\beta^2 d + k_m^2\,[\,[1 + d]\,S - \alpha\,[d\,f_u + g_v]]\;\beta_D\; + \left[\alpha^2[f_u\,g_v - f_v\,g_u] - \alpha\,[f_u + g_v]\,S + S^2\right] < 0, \tag{S.37}$$

which, given the condition for stability (S.34), can be simplified to

$$[1 + d]\,S - \alpha\,[d\,f_u + g_v] < 0. \tag{S.38}$$

This relation provides a necessary condition but is not sufficient on its own. To establish a condition that is both necessary and sufficient, the minimum value $h(k_m^2)$ must be negative. This leads to the following condition

$$\frac{1}{4d}\,(\,[1 + d]\,S - \alpha\,[d\,f_u + g_v])^2 - \left[\alpha^2|\mathbb{A}| - \alpha\,tr(\mathbb{A})\,S + S^2\right] > 0. \tag{S.39}$$

Instability zone

The range of values k_m^2 for which $h(k_m^2)$ is negative is

$$2\beta_D d\, k_{1,2}^2 = [\ \alpha\ [d\ f_u + g_v] - [1+d]S\ ] \mp \sqrt{(\alpha\ [d\ f_u + g_v] - [1+d]S)^2 - 4d\,[\alpha^2|\mathbb{A}| - \alpha\ tr(\mathbb{A})\ S + S^2]}. \tag{S.40}$$

In two dimensions, in a rectangular domain $L_x(t) \times L_y(t)$ the condition becomes

$$k_1^2 < k_{nm} = \left(\left(\frac{n}{L_x}\right)^2 + \left(\frac{m}{L_y}\right)^2 \right)^2 \pi^2 < k_2^2, \tag{S.41}$$

with n and m positive integers. It can be verified that for $S = 0$ (absence of growth), the standard conditions are recovered [44].